Effect of Dopants on Grain Coalescence and Oxygen Mobility in Nanostructured Titania Anatase and Rutile

V. Guidi,*,† M. C. Carotta, M. Ferroni, and G. Martinelli

Dipartimento di Fisica and INFM, Via Paradiso 12, I-44100 Ferrara, Italy

M. Sacerdoti

Dipartimento di Scienze della Terra, Corso Ercole I d'Este 4, I-44100 Ferrara, Italy

Received: September 19, 2001; In Final Form: October 9, 2002

Grain growth and the anatase-to-rutile phase transition in nanostructured titania have been investigated by electron microscopy, X-ray diffraction, and differential thermal analysis. For pure TiO_2, thermal treatment resulted in complete phase transition and considerable grain coarsening, because of the grain boundary nucleation mechanism for the rutile phase. The effect of doping of the TiO_2 nanophase has also been addressed. Phase transition turned out to be strongly affected by the presence of Ta and Nb because nucleation of rutile was favored at the surface of anatase grains. Doping allowed the maintenance of the ultrafine anatase phase even at high annealing temperature. Thermal analysis highlighted that oxygen mobility in the titania lattice is affected by doping and related to the inhibition of grain coalescence and phase transition.

Introduction

Titania films possess an immense range of applications, e.g., in the field of optics,[1] electrical insulation,[2] photovoltaic solar cells,[3,4] electrochromic displays,[5] antibacterial coatings,[6] photocathalitic reactors,[7] high-performing anodes in ion batteries,[8] and gas sensing.[9] In the nanometric domain, titania revealed unexpected properties because of the increased fraction of atoms located at the surface or at the grain boundaries. The production of titania films featuring nanometric grain sizes opens up a new field of research, and currently, some applications have greatly benefited from a nanostructured phase for TiO_2.[10,11] Indeed, some methods for the achievement of nanostructured thin or thick titania films were recently proposed.[12−14] As a remarkable example, the field of gas sensing has taken advantage of titania-nanostructured films for chemoresistive gas detection with improved sensitivity.[15]

Presently, a big effort is dedicated to understanding the basic properties of nanometric titania, with particular emphasis on the mechanisms that lead to stabilization of the layers. Anatase and rutile are the most interesting phases for titania. At room temperature, rutile is the stable arrangement of atoms although anatase can easily exist or coexist in a metastable state because of a little enthalpy difference, $\Delta H_{tr} = -62.5$ J/g.[16,17] On heating, anatase irreversibly transforms into rutile with a moderate exothermic contribution. As reported in the literature, the phase transition occurs at a temperature between 400 and 1200 °C.[18] However, it was recently demonstrated that a very low particle size (below 14 nm) causes the anatase phase to be thermodynamically stable.[19] The evolution of titania films upon annealing has been extensively studied, indicating that grain growth is affected by several parameters such as porosity and the anatase-to-rutile phase transition.[20−22]

This work will address the effects of dopant addition on the microstructural evolution of a TiO_2-based nanostructure through a combined structural and thermal analysis. The experimental observation highlights the way that the presence of impurities in the titania lattice affects the ionic mobility, resulting in effective grain coalescence inhibition and hindering of the anatase-to-rutile phase transition. This basic knowledge will improve the capability to produce stable layers of nanostructured TiO_2.

Experimental Section

Nanometric powders of pure and doped titania produced by laser-assisted pyrolysis[23] or the sol−gel technique[24] have been investigated. These preparation methods allow one to achieve nanometric-sized particles with narrow distribution of grain dimension. Commercially available powders do not fulfill such a requirement.

The TiO_2 powders have been characterized as both dispersed powders and sintered films. Deposition of the films was carried out through a screen-printing apparatus (for details, see ref 13). Firing at various temperatures in controlled airflow accomplished the preparation. Oxidation was carried out in a furnace under controlled flux of synthetic air as follows: the temperature was raised to a nominal temperature—ranging from 400 to 1100 °C—at 20 °C/min, maintained at this level for 1 h, and finally decreased to room temperature at 2 °C/min.

Doping with Nb, Ta, and Ga was considered in the 3−11% weight range. We performed the addition with such dopants because of their ionic radii, which are similar to that of Ti (see Table 1). This would favor the substitution of Ti ions in the titania lattice and result in different electrical properties. As reported in ref 25, Nb and Ta substitute Ti sites in titania, yielding *n*-doping, in contrast to Ga that causes *p*-doping.

Structural characterization was performed over powders and sintered films by scanning or transmission electron microscopy

* To whom correspondence should be addressed. Tel: +39-0532974284. Fax: +39-0532974210. E-mail: guidi@fe.infn.it.

† Also affiliated with INFN Sezione di Ferrara.

10.1021/jp013572u CCC: $25.00
Published on Web 12/07/2002

TABLE 1: Ionic Radius of the Dopant Added to Titania[a]

element	ionic radius (Å)	element	ionic radius (Å)
Ti^{4+}	0.61	Nb^{5+}	0.64
Ga^{3+}	0.62	Ta^{5+}	0.65

[a] The value for Ti in six-fold coordination is indicated for comparison.

TABLE 2: Summary of Results on Annealing of Powders Flowed in N_2 Atmosphere

preparation	doping	initial rutile (%)	ΔH (J/g)	T_{peak} (°C)
pyrolysis	none	0	320 ± 30	840 ± 10
	Nb (3%)	2	390 ± 30	930 ± 10
	Nb (11%)	14	400 ± 30	960 ± 10
	Ga (11%)	15	250 ± 30	890 ± 10
	Ta (11%)	22	210 ± 30	940 ± 10
sol−gel	none	0	145 ± 15	780 ± 10
	Nb (5%)	0	135 ± 15	850 ± 10
	Nb (10%)	0	180 ± 15	840 ± 10
	Ta (5%)	0	155 ± 15	860 ± 10
	Ta (10%)	0	130 ± 15	880 ± 10

(SEM or TEM) and X-ray diffraction (XRD). Differential thermal analysis (DTA) on the powders, assisted by thermogravimetry, was also carried out.

A Cambridge 360 scanning electron microscope with energy dispersive X-ray spectroscopy microanalysis and a Hitachi H-800 transmission electron microscope were operated at 30 and 200 kV, respectively. For TEM characterization, titania films were deposited over a monocrystalline (100)-oriented Si substrate. Sample preparation was performed by low-angle ion milling. Bright field images and selected area electron diffraction (SAED) patterns were recorded; the ordered lattice of Si was used for TEM calibration, which allowed precise determination of the lattice parameters of the samples.

XRD measurements were performed in the Bragg−Brentano geometry by a powder diffractometer operating with monochromatic Cu Kα radiation. DTA was carried out using a Netzch STA-409 analyzer. Measurements were carried out in the temperature range of 400−1100 °C in either nitrogen, argon, or helium flow at a 20 °C/s heating rate.

Results and Discussion

Morphological and Structural Characterization. The characterization will primarily address the phenomena of grain growth and phase transition occurring in the nanophase and the effect caused by dopant addition. Figure 1 (left and center) illustrates the morphology of the undoped powders after heating at 400 or 1100 °C. Both samples consisted of an homogeneous polycrystalline nanostructure, and the distributions of particle size for the two samples, reported in Figure 1 (right), clearly indicate that considerable grain coalescence occurred during annealing. SAED as well as XRD patterns showed that the powders fired at 400 °C were formed by TiO_2 anatase. Differently, SAED indicated that nearly a complete conversion of anatase into rutile was promoted by firing at 1100 °C.

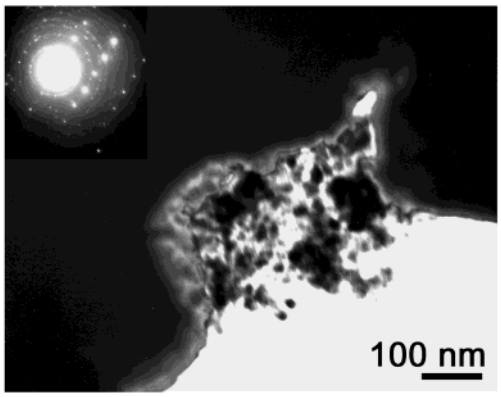

Figure 2. TEM image and the relative SAED pattern (inset) of the sample fired at 1100 °C. The image highlights a small cluster of TiO_2−anatase particles surrounded by large TiO_2−rutile grains. The rings and the systematic rows in the SAED pattern indicate that the small grains and the large particles are in the anatase and rutile phase, respectively.

Investigation by TEM highlighted a relationship between grain growth and the anatase-to-rutile phase transition. Figure 2 shows the presence of a cluster of tiny particles surrounded by large grains in the sample fired at 1100 °C. The large grains turned out to be in the rutile phase. Differently, the small particles of the cluster were TiO_2 anatase and their average size (24 nm) was close to the value measured in the sample fired at 400 °C (19 nm); that is, no appreciable grain growth occurred for these anatase particles. The increase in grain size appears to be assisted by the anatase-to-rutile phase transition, which increased the atom mobility by breaking some Ti−O bonds in the titania lattice.[21]

The effect of different dopings on grain growth in TiO_2 is reported in Figure 3. Grain coarsening in Ta-doped and—to some extent—in Nb-doped samples was effectively inhibited over a relatively wide temperature range. Differently, an abrupt increase in grain size for the Ga-doped powders occurred above 650 °C. Measurement of grain size indicated that the evolution of the Ga-doped samples was similar to that of the undoped TiO_2 powders.

Figures 4 and 5 highlight the phenomenon of grain growth for the Ga-doped sample. In particular, Figure 5 shows a large TiO_2 grain, achieved by firing at 1100 °C, from which the

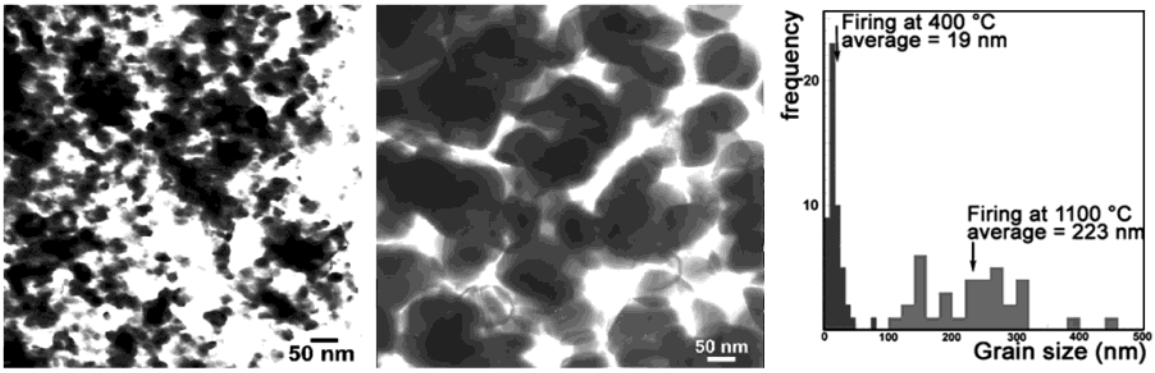

Figure 1. TEM images of the undoped film of TiO_2 after thermal treatment: sample fired at 400 °C (left), sample fired at 1100 °C (center), and grain size distribution for the two samples (right).

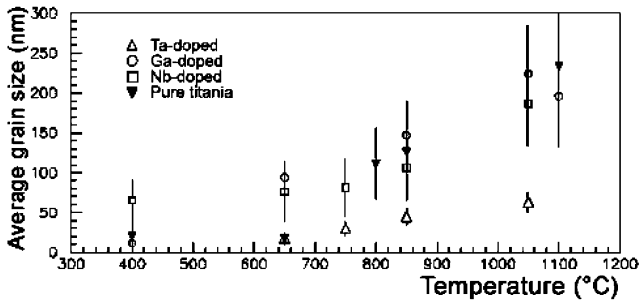

Figure 3. Average grain size as a function of temperature for pure and doped titania films as measured by SEM and TEM. The uncertainties were calculated as root mean square values of the grain size distributions.

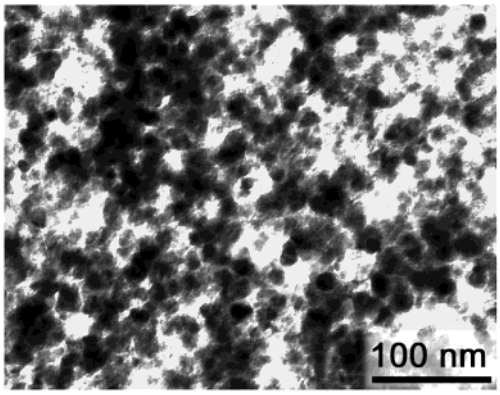

Figure 4. TEM image of the sample doped with Ga after firing at 400 °C.

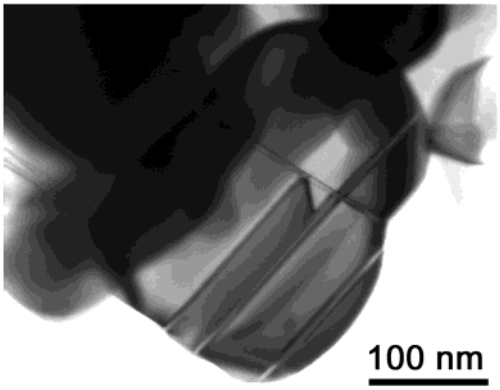

Figure 5. TEM image of a large rutile particle formed in the Ga-doped film after firing at 1100 °C. The morphology suggests that formation of particle occurred from boundary nucleation of rutile at the interface between several anatase particles.

mechanism of coarsening can be inferred; clearly visible defects across the whole particle indicate that some grains of anatase have merged into the TiO_2 rutile particle.

Experimental evidence indicates that grain coalescence and phase transition in TiO_2 were affected by the presence of dopants. Anatase can indeed be conceived as an arrangement of parallel Ti−O octahedra while for rutile some of the octahedra are rotated by 90°.[26−28] Thereby, conversion from anatase to rutile can be regarded in terms of rearrangement of octahedra orientation,[29] with a symmetry change from the $I4_1/amd$ to $P4_2/mnm$ space group. Ta and Nb stabilized the nanosized structure of titania because they were substitutionally soluted in the TiO_2 lattice. The presence of a dopant or a compound in a nanograined structure can affect the rate of grain growth and the density of rutile nucleation sites via two basic mechanisms: (i)

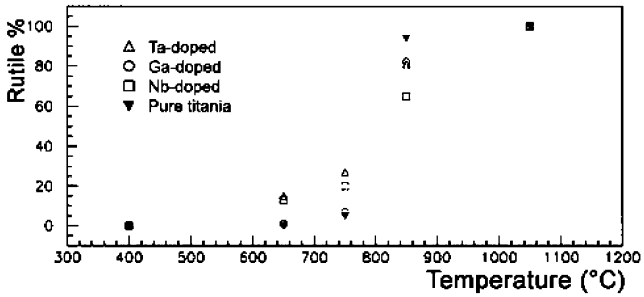

Figure 6. Percentage of rutile nucleated from anatase as a function of temperature for pure and doped titania films. The percentage is normalized to the initial content of anatase.

segregation at the grain boundary of a phase lowering the superficial energy of the grains or (ii) occupation of bulk lattice sites in such a way to hinder the ionic mobility. Extended X-ray absorption fine structure measurements actually indicated the substitution of Ti lattice sites by Ta.[30] In the case of Nb, measurements were carried out over samples doped at 3 and 11% weight ratio. Nb in the 3% sample was demonstrated to be substitutionally soluted in the TiO_2 lattice,[31] irrespective of the firing temperature. Differently, the 11% doped film revealed the presence of some percent of Nb_2O_5 and Nb_2TiO_7.[32,33] XRD analysis also showed that such a Nb−Ti oxide did not account for the whole content of Nb. Probably, the remaining Nb was soluted in the TiO_2 lattice at the solubility limit, which is reported to be about 5%.[34] However, both samples doped with Nb featured comparable inhibition to grain growth, indicating that segregation of the mixed oxide at high temperature did not affect the evolution of the nanostructure. In summary, there is an indication that Ta and Nb are effective in preventing grain growth because of the substitution of Ti sites in the lattice and of the consequent reduction of ionic mobility.

The anatase-to-rutile phase transition of titania vs annealing was extensively studied by XRD. Anatase and rutile proportions were measured through Rietveld refinement of the XRD patterns of both phases.

Just after preparation, pure titania powders prepared by a spray pyrolysis methodology were in anatase phase while the doped powders were partially in rutile phase. Differently, the powders prepared by sol−gel were in anatase phase only.[34] Figure 6 shows that the conversion basically occurred within 750−850 °C for the samples prepared by spray pyrolysis. Phase transformation was nearly accomplished for the pure TiO_2 sample within this temperature range, while that was not the case for Nb and Ta dopings. Ga-doped titania featured a transformation of 75% anatase into rutile, and the percentage of conversion was about 45% and 50% for the Nb- and Ta-doped samples, respectively.

As far as the sol−gel-prepared powders are concerned, no significant change in the onset of phase transition and also grain coarsening was recorded with respect to the samples prepared by spray pyrolysis. XRD analysis highlighted that firing of the doped films at intermediate temperature resulted in a TiO_2 nanostructure, where both anatase and rutile were present. It came out a bimodal size distribution, indicating the presence of small and large grains, supporting the hypothesis that the increase in grain size is assisted by phase transition.

It has been reported in the literature that nucleation of rutile occurs at either grain's surface, at the boundary among particles, or in the bulk.[35] In particular, boundary nucleation results in significantly larger rutile particles, because one or more anatase grains are merged into a single rutile grain. Rutile nucleation

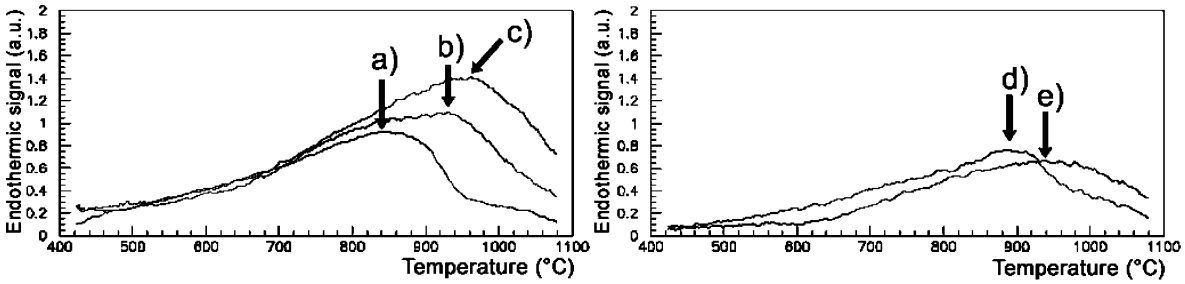

Figure 7. Variation of DTA signal corresponding to irreversible endothermic transformation to the powders produced through pyrolysis. Arrows mark the maxima of the endothermic curves: (a) undoped, (b) Nb added (3%), (c) Nb added (11%), (d) Ga added, and (e) Ta added.

within anatase bulk grains requires a higher activation energy and therefore would occur at higher temperature.

The observed sharp increase in grain size vs temperature for pure titania powders indicates that nucleation of rutile occurred at the boundary of the grains, consistent with the results reported in ref 18 for the same temperature range. In contrast, phase transition was a gradual process for the Nb- and Ta-doped samples, starting at temperatures lower than 600 °C and extending at higher temperatures. TEM observation about the morphology of the Nb- and Ta-doped TiO_2 particles after high-temperature firing did not reveal the presence of large rutile grains (similar to the one shown in Figure 5) as a result of the union of some anatase grains. This record does not support the hypothesis of boundary nucleation as the leading mechanism for rutile nucleation in Nb- and Ta-doped powders. Instead, such evidences, combined with the low onset temperature recorded for the phase transition, would indicate a surface nucleation mechanism for the Nb- and Ta-doped powders. Such a mechanism is accompanied by an increased density of rutile nucleation centers resulting in a limitation to the average size of the rutile particles, as experimentally observed.

Thermal Characterization. Thermal analysis was carried out over the films in order to investigate the effect of Ta, Nb, and Ga dopings on the ionic mobility in titania. Titania is known to possess a high diffusion coefficient for oxygen ions above 500 °C.[36] Therefore, the execution of DTA measurements over the powders under nitrogen or argon flux would yield precious information about oxygen mobility in the lattice. Thus, any retardation or stimulation in the flux of oxygen from the bulk into the gaseous phase could be correlated to oxygen mobility and indirectly to grain growth and phase transition onset.

The powders were first heated at 600 °C for 1 h in order to evaporate chemisorbed water and then slowly decreased to 400 °C. Then, the samples were repeatedly heated and cooled from 400 to 1100 °C at moderate temperature rate (±20 °C/min). From the second cycle on, we observed that the thermal signal did not change appreciably. Thus, the difference in the DTA signal of the second stage to the first one highlighted the irreversible transformations that occurred during the first stage (Figure 7). It resulted in a broad endothermic curve roughly extending within 500−1000 °C. The area below the curves is a measure of the corresponding enthalpy variation, ΔH. After calibration with sapphire powders, we determined the values of ΔH, as summarized in Table 2. In addition, thermogravimetric measurements showed that during the first heating, the powders suffered a considerable weight loss (5−7%).

Repetition of the measurements at a slower heating/cooling rate (±10 and ±5 °C/min) did not highlight any difference, nor did the gas (N_2 or Ar) where the powders were fluxed make a change. Thus, after the first heating cycle, the powders can be regarded as stabilized. Such evidence was confirmed by XRD and TEM analyses, which indicated that the duration of the thermal treatment was sufficient to guarantee the stability of the microstructure. Indeed, longer thermal treatments (up to 20 h) did not significantly affect the grain size and morphology of the samples. The stability of the powders as printed layers was profitably used for high-temperature gas sensing with long-term operation.[11,24,25]

A closer analysis of Figure 7 shows that the temperature corresponding to the maximum of the endothermic curves was found to depend on the presence of a dopant. Table 2 also encompasses the position of such maxima. In particular, the pure powders exhibited the lowest temperature at which the maximum was attained. It is also evident that the shift of the maximum toward higher temperature was recorded for the samples that highlighted the greatest coalescence inhibition.

The endothermic nature of the observed curve looks considerably surprising. One would expect all of the involved phenomena to be exothermic: primarily coalescence and phase transition, as well as strain relaxation, lattice repair, or surface adsorption. An analogous circumstance about titania nanopowders has been reported in the literature[37] and interpreted in terms of desorbtion of physisorbed and chemisorbed water occurring below 600 °C. However, in our case, Fourier transform infrared measurements completely discarded this occurrence.

The interpretation of the endothermic curve is as follows: at elevated temperatures, oxygen ions in the lattice possess considerable mobility and thus diffuse toward and from the surface. Therefore, oxygen is endothermically desorbed and exothermally adsorbed with the same rate at equilibrium. In our case, DTA measurements were executed under Ar or N_2 flux so that only endothermic desorption was allowed. The energy for breaking the Ti−O bond is considerable; therefore, the endothermic contribution was so high as to dominate all other exothermic processes involved. Thus, the position of the thermal peak is bound up to oxygen desorption and, in turn, to oxygen mobility.

We observed a correlation between the samples for which coalescence and phase transition are inhibited and those exhibiting the largest temperature shift in the maximum of the DTA curve. Therefore, it appears clear that the introduction of a dopant decreases oxygen mobility and then retards oxygen desorption. On the strength of this evidence, it is highly reasonable that the mechanism responsible for grain growth inhibition is a modification of oxygen mobility rather than a superficial tension effect.

Conclusions

In this work, we have shown that stabilization of nanostructured TiO_2 films is possible by proper doping. In particular, Ta and Nb dopings proved effective to prevent grain coalescence

below 850 °C. This finding is important for all applications in which a titania film is needed to be maintained as a nanostructured phase.

The anatase-to-rutile phase transition was demonstrated to affect the final grain size of the layers. For pure titania, rutile formation preferentially occurred via boundary nucleation, resulting in significant grain coarsening. Differently, the presence of Nb or Ta appeared to favor the mechanism of surface nucleation for rutile, leading to a slower process, which in turn prevented exaggerated grain growth.

Thermal measurements highlighted the diffusion of oxygen in the TiO_2 lattice, which was affected by dopants. Ta- and Nb-doped samples shifted the DTA peak toward higher temperatures—a confirmation for the decrease in oxygen mobility. On the basis of this evidence, the inhibition to grain coalescence is ascribed to a decrease in ionic mobility.

References and Notes

(1) Tang, H.; Prasad, K.; Sanjinés, R.; Lévy, F. *Sens. Actuators B* **1995**, *26/27*, 71.
(2) Bange, K.; Ottermann, C. R.; Anderson, O.; Jeschkowsky, U.; Laube, M.; Feile, R. *Thin Solid Films* **1991**, *197*, 279.
(3) O'Regan, B.; Grätzel, M. *Nature* **1991**, *353*, 737.
(4) Gerfin, T.; Grätzel, M.; Walder, L. *Prog. Inorg. Chem.* **1997**, *44*, 345.
(5) Marguetettaz, X.; Fitzmaurice, D. *J. Am. Chem. Soc.* **1994**, *116*, 5017.
(6) Sunada, K.; Kikuchi, Y.; Hashimoto, K.; Fujishima, A. *Environ. Sci. Technol.* **1998**, *32*, 726.
(7) For a complete view on this topic, see *Proceedings of the Third International Conference on TiO_2 Purification and of Water and Air*; Al-Ekabi, H., Ed.; Orlando, 1997.
(8) Huang, S. Y.; Kavan, L.; Exnar, I.; Grätzel, M. *J. Electrochem. Soc.* **1995**, *142*, L142.
(9) Ferroni, M.; Guidi, V.; Martinelli, G.; Nelli, P.; Sberveglieri, G. *Sens. Actuator B* **1997**, *44*, 499.
(10) Beck, D. D.; Siegel, R. W. *J. Mater. Res.* **1992**, *7*, 2840.
(11) Ferroni, M.; Faglia, G.; Guidi, V.; Nelli, P.; Martinelli, G.; Sberveglieri, G. *Nanostruct. Mater.* **1996**, *7*, 709.
(12) Bally, A. R.; Korobeinikova, E. N.; Schmid, P. E.; Lévy, F.; Bussy, F. *J. Phys. D: Appl. Phys.* **1998**, *31*, 1149.
(13) Carotta, M. C.; Ferroni, M.; Guidi, V.; Martinelli, G. *Adv. Mater.* **1999**, *11*, 943.
(14) Guidi, V.; Carotta, M. C.; Ferroni, M.; Martinelli, G.; Paglialonga, L.; Nelli, P.; Sberveglieri, G. *Sens. Actuators B* **1999**, *57*, 197.
(15) Sberveglieri, G.; Depero, L. E.; Ferroni, M.; Guidi, V.; Martinelli, G.; Nelli, P.; Perego, C.; Sangaletti, L. *Adv. Mater.* **1996**, *8*, 334.
(16) Fahmi, A.; Minot, C.; Silvi, B.; Causà, M. *Phys. Rev. B* **1993**, *47*, 11717.
(17) *Handbook of Chemistry and Physics*; West, R. C., Ed.; CRC: Cleveland, 1986.
(18) Gouma, P. I.; Dutta, P. K.; Mills, M. J. *Nanostruct. Mater.* **1999**, *11*, 1231.
(19) Zhang, H.; Banfield, J. *J. Mater. Chem.* **1998**, *8*, 2073.
(20) Ding, X.; Liu, X. *J. Mater. Res.* **1998**, *13*, 2556.
(21) Zhang, H.; Banfield, J. *Am. Mineral.* **1999**, *84*, 528.
(22) Mayo, M. J.; Hague, D. C. *Nanostruct. Mater.* **1993**, *3*, 43.
(23) Depero, L. E.; Sangaletti, L.; Bontempi, E.; Salari, R.; Zocchi, M.; Casale, M. C. *J. Mater. Res.* **1998**, *13*, 1644.
(24) Traversa, E.; Di Vona, M. L.; Licoccia, S.; Sacerdoti, M.; Carotta, M. C.; Gallana, M.; Martinelli, G. *J. Sol−Gel Sci. Technol.* **2000**, *19*, 193.
(25) Bonini, N.; Carotta, M. C.; Chiorino, A.; Guidi, V.; Malagù, C.; Martinelli, G.; Paglialonga, L.; Sacerdoti, M. *Sens. Actuators B* **2000**, *68*, 274.
(26) Eastman, J. A. *J. Appl. Phys.* **1993**, *75*, 770.
(27) JCPDS PDF-2 pattern 21-1272.
(28) JCPDS PDF-2 pattern 21-1276.
(29) Moslay, P. T. *Sens. Actuator B* **1992**, *6*, 149.
(30) Cavicchi, B.; Danconi, M. C.; Ferroni, M.; Sacerdoti, M. Unpublished results.
(31) Ferroni, M.; Carotta, M. C.; Guidi, V.; Martinelli, G.; Ronconi, F.; Richard, O.; Van Dyck, D.; Van Landuyt, J. *Sens. Actuators B* **2000**, *68*, 140.
(32) JCPDS PDF-2 pattern 30-0873.
(33) JCPDS PDF-2 pattern 39-1407.
(34) Eror, N. G.; Smyth, D. M. In *Proceedings of the Advanced Study on the Chemistry of Extended Defects in Non-Metallic Solids*; Eyring, L., Keeffe, M. O., Eds.; North-Holland: Amsterdam, 1970; p 71.
(35) Zhang, H.; Banfield, J. *J. Mater. Res.* **2000**, *15*, 437.
(36) Kirner, U.; Schierbaum, K. D.; Göpel, W.; Leibold, B.; Nicoloso, N.; Weppner, W.; Fischer, D.; Chu, W. F. *Sens. Actuators B* **1990**, *1*, 103.
(37) Tan, M.; Wang, G.; Zhang, L. *J. Appl. Phys.* **1996**, *80*, 1186.